IRSTI 27.35.21; 27.35.47; 27.41.19 https://doi.org/10.26577/ijmph.202516210

A.A. Issakhov[1*], U. Timokhina[2], J. Na[2], Zh. Batyrbekova[2], Zh. Makasheva[2], A. Akylova[2], D. Tokbayev[2]

[1]Kazakh-British Technical University, Almaty, Kazakhstan
[2]International School Haileybury, Almaty, Kazakhstan
*e-mail: alibek.issakhov@gmail.com
(Received 24 August 2025; accepted 31 October 2025)

CFD study of the effect of coarctation on the distribution of velocities, pressures, and shear stresses in the thoracic aorta

Abstract. This study focuses on numerical modeling of thoracic aortic hemodynamics in patients with coarctation, a congenital narrowing of the vessel lumen that impairs blood flow and increases hemodynamic load. The aim of the study was to identify the influence of geometric changes in the aorta on the distribution of velocity, pressure, and shear stress using computational fluid dynamics (CFD) methods. The mathematical model is based on the Navier-Stokes equations for an incompressible non-Newtonian fluid, which describes the rheological properties of blood. Calculations were performed using the finite volume method with an explicit time-dependent scheme for two geometric configurations – normal and pathological. Analysis of the resulting velocity and pressure fields revealed that with coarctation, the maximum velocity increases by approximately 1.6 times, and the pressure difference between the ascending and descending aorta reaches 0.6 kPa. The shear stress distribution revealed localized areas of extreme values that potentially contribute to endothelial dysfunction. This study contributes to the development of personalized blood flow modeling and demonstrates the potential of CFD methods for assessing hemodynamic disturbances in vascular pathologies, which has practical implications for preliminary diagnosis and treatment planning.
Keywords: hemodynamics, coarctation of the aorta, computational fluid dynamics, CFD, numerical modeling.

Introduction

Coarctation of the aorta (CoA) is a congenital narrowing of the thoracic aorta that impedes normal blood flow and causes compensatory redistribution through collateral vessels. This leads to arterial hypertension in the upper body, left ventricular overload, and left ventricular hypertrophy [1, 2]. Despite the advancement of surgical correction techniques and catheter-based interventions, the risks of recoarctation and aneurysm formation remain, which are associated with local hemodynamic disturbances [3]. Therefore, increasing attention is being paid to methods for quantitative assessment of blood flow parameters that can identify key biomarkers of the disease.

One rapidly developing area is the use of phase-contrast magnetic resonance imaging (4D flow). This method allows for obtaining spatiotemporal velocity distributions, assessing pressure differences, and wall shear stress (WSS), which has high diagnostic value [4]. Studies have shown that 4D flow can be used to identify pathological changes in blood flow and assess the effectiveness of surgical treatment [5–7]. However, limitations of the method relate to spatial and temporal resolution, noise, and distortions arising from tissue movement and magnetic field properties, which reduce the accuracy of the data obtained [40].

Numerical methods are increasingly being used to improve the reliability of analysis. Combining clinical data with computational modeling allows for a detailed understanding of hemodynamics and the assessment of parameters difficult to measure directly [8, 9]. In this context, computational fluid dynamics (CFD) methods have gained a special place, as they enable the reproduction of velocity fields, pressure distributions, and WSS in individual vessel geometries. Unlike traditional clinical measurements, CFD provides a three-dimensional description of flows and allows for the investigation

of the influence of both geometric features and boundary conditions [10–12].

High WSS values are associated with endothelial damage, while low values create conditions favorable for atherogenesis [13, 14]. LaDisa et al. [10] demonstrated that changes in geometry after surgical correction of CoA lead to significant restructuring of the WSS distribution and the formation of zones with increased risk of atherosclerotic lesions. Similar conclusions were reached in other studies, where local hemodynamic characteristics were considered as a determining factor in further disease progression.

The literature also contains studies using more complex simulations that take into account the interaction of blood and the vessel wall (Fluid-Structure Interaction, FSI). Such models are capable of accounting for aortic deformation under the influence of pulsatile flow [12, 15–18]. Including wall compliance has been shown to provide a more accurate match to clinical data; however, it requires significantly greater computational resources and detailed information on the mechanical properties of tissues. Therefore, CFD remains a fundamental tool for hemodynamic studies and is widely used to analyze pathologies, including coarctation of the aorta.

Despite a significant amount of research, the influence of the degree and shape of stenosis on the spatiotemporal distribution of velocity, pressure, and shear stress in the thoracic aorta remains insufficiently quantitatively described. This study numerically simulates hemodynamics in the thoracic aorta using anatomically realistic geometry derived from medical images. Two models are considered: a normal aorta and an aorta with coarctation. The focus is on analyzing the distribution of velocities, pressures, and wall shear stress, which allows us to identify characteristic features of blood flow and assess the impact of stenosis on key hemodynamic parameters.

Materials and Methods

Mathematical Model

Blood flow in the thoracic aorta is described by the Navier-Stokes equations for an incompressible fluid. Blood is assumed to be a non-Newtonian fluid with a constant density of $\rho = 1050$ kg/m³.

Continuity equation:

$$\nabla \cdot u = 0 \tag{1}$$

Momentum equation:

$$\rho\left(\frac{\partial u}{\partial t} + u \cdot \nabla u\right) = -\nabla p + \nabla \cdot \tau \tag{2}$$

where:

u – is the velocity vector, m/s;

p – is the pressure, Pa;

τ – is the viscous stress tensor, Pa.

To describe the viscosity properties of blood, the Carreau rheological model is used, which accurately reflects the behavior of blood in arterial flow [19, 20]:

$$\mu(\dot{\gamma}) = \mu_\infty + (\mu_0 - \mu_\infty)[1 + (\lambda\dot{\gamma})^2]^{\frac{(n-1)}{2}} \tag{3}$$

where:

$\mu_0 = 0.056$ Pa s is the viscosity at zero shear rate;

$\mu_\infty = 0.00345$ Pa s is the viscosity at infinite shear rate;

$n = 0.3568$ is the exponent;

$\lambda = 3.313$ s is the time parameter;

$\dot{\gamma}$ – is the effective shear rate, s^{-1}.

Boundary conditions

A pulsatile velocity profile (Fig. 1a) was defined at the entrance to the ascending aorta, reconstructed from clinical measurements. The cardiac cycle period was T = 0.75 s, with the maximum velocity during systole reaching 0.6 m/s. The profile was approximated using 119 points and interpolated according to the time step. Free-flow conditions (p = 0) were defined at the exits of the thoracic aorta, carotid, and subclavian arteries. The aortic walls were treated as rigid boundaries.

Numerical Method

The equations were solved using the finite volume method. The SIMPLE algorithm was used to relate pressure and velocity [26, 27]. Convective terms were approximated by a second-order wind-dependent scheme, and diffusion terms were approximated by a second-order scheme. An explicit scheme with a step size of $\Delta t = 0.005$ s was used for time discretization. The maximum number of internal iterations at each time step was limited to 20.

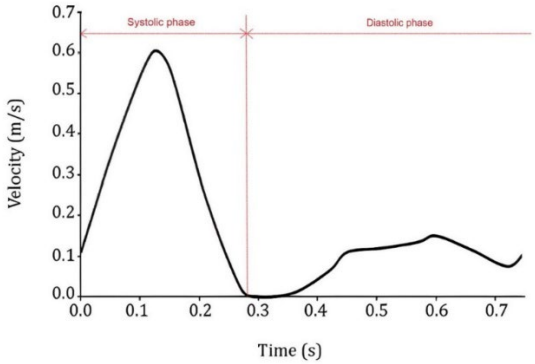

Figure 1 – Inlet velocity boundary condition

Geometry and Mesh

Thoracic aortic geometries were reconstructed from medical images from an open database [21]. Two cases were considered: a normal aorta and an aorta with coarctation in the region between the left carotid and subclavian arteries. Model preparation and cleaning were performed using SpaceClaim and Design Modeler.

A tetrahedral mesh was constructed for numerical calculations. A sensitivity analysis to element size was performed: three meshes with characteristic cell sizes of 1 mm, 2 mm, and 3 mm were considered. Mesh parameters are listed in Table 1.

A comparison of the average velocity time profiles for the three mesh variants is shown in Figure 2. The results showed that when switching from 2 mm to 1 mm, the velocity discrepancy was less than 0.005 m/s, indicating sufficient mesh convergence. Based on this, a mesh with an element size of 2 mm was selected for all subsequent calculations as it provided the optimal balance between accuracy and computational cost. Figure 3 shows the final mesh for normal and pathological geometries.

Table 1 – Parameters of computational grids for sensitivity analysis

Mesh no.	Mesh size	Element number	Velocity (m/s)
mesh 1	3 mm	196,805	0.3965
mesh 2	*2 mm*	*663,385*	*0.3971*
mesh 3	1 mm	5,284,194	0.4005

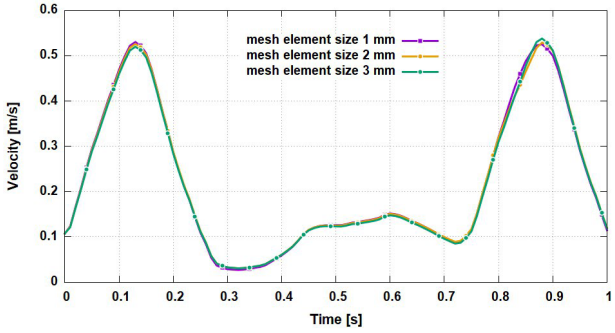

Figure 2 – Comparison of velocity profiles obtained on three grid variants

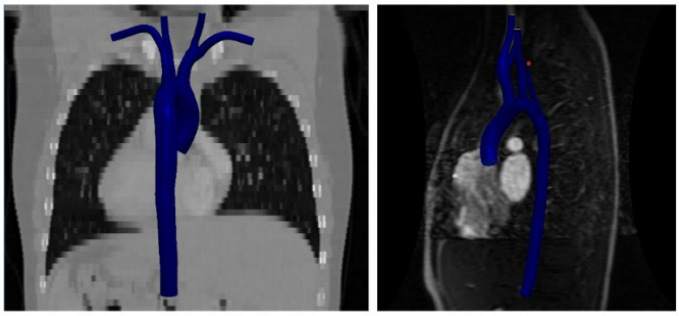

a)

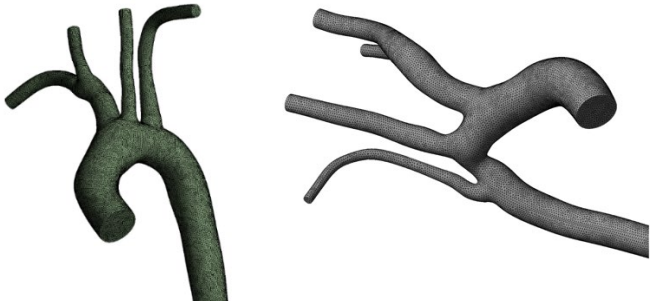

b

Figure 3 – Geometries (a) and computational grids (b):
on the left – aorta without pathology, on the right – aorta with coarctation

Numerical Model Validation

To verify the validity of the selected numerical methods, a test simulation of unsteady Poiseuille flow under laminar conditions (Re = 100) was performed in a circular pipe of constant diameter D = 0.01 m and length L = 0.1 m. Water with a density of 998 kg/m^3 and a constant viscosity of 0.001003 kg/(m s) was used as the working fluid.

A comparison of the calculated velocity profiles in two cross-sections (x/L = 0 and x/L = 0.9) with the analytical solution showed satisfactory agreement (Figure 4). The results confirm that the chosen numerical scheme and spatial discretization correctly reproduce classical solutions and can be used to model blood flow in the aorta.

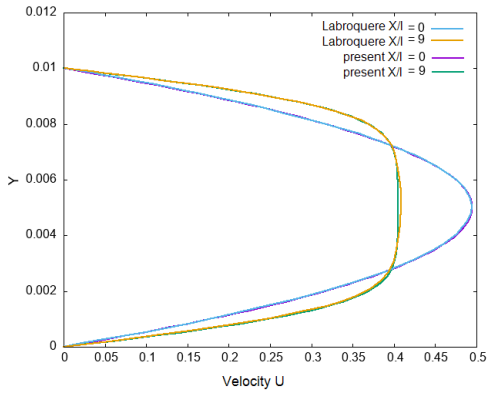

Figure 4 – Comparison of velocity profiles for unsteady Poiseuille flow:
numerical solution, analytical distribution and numerical results of Labroquere [22]

Results and Discussion

Velocity Distribution

Figure 5 shows the velocity distribution in the aorta without pathology and with coarctation at characteristic moments of the cardiac cycle—peak systole and late diastole. In a normal aorta, the flow maintains an axisymmetric structure, with maximum velocities reached in the central part of the lumen. With coarctation, marked blood flow acceleration is observed in the narrowing zone, with the formation of a jet flow.

After the narrowing zone, an extended section with a high velocity gradient and pronounced turbulence develops. This is accompanied by the appearance of reverse flow zones in the descending aorta, particularly noticeable at the end of systole. This flow pattern differs significantly from a laminar profile and is consistent with clinical observations of hemodynamic disturbances associated with coarctation.

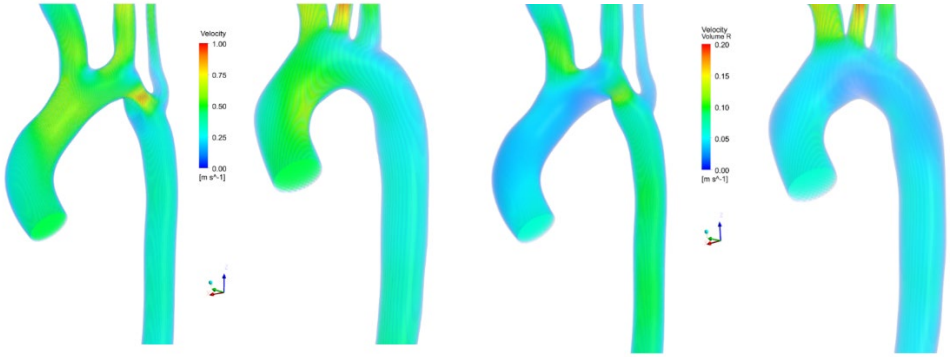

a b

Figure 5 – Velocity field in the normal aorta and with coarctation:
a – peak systole, b – end diastole

The average velocity time profiles in the ascending and descending aorta for both cases are shown in Figure 6. In a normal aorta, the velocity profile is smooth, while with constriction, the amplitude of oscillations increases significantly. The maximum velocity in the coarctation zone exceeds the corresponding values for a normal aorta by more than 1.6 times, confirming the presence of significant hemodynamic loading on the vessel walls.

Analysis of the dynamics showed that the difference between normal and pathological geometry is most pronounced during peak systole. During diastole, the differences smooth out, but the jet-like nature of the flow beyond the coarctation zone persists throughout the cycle.

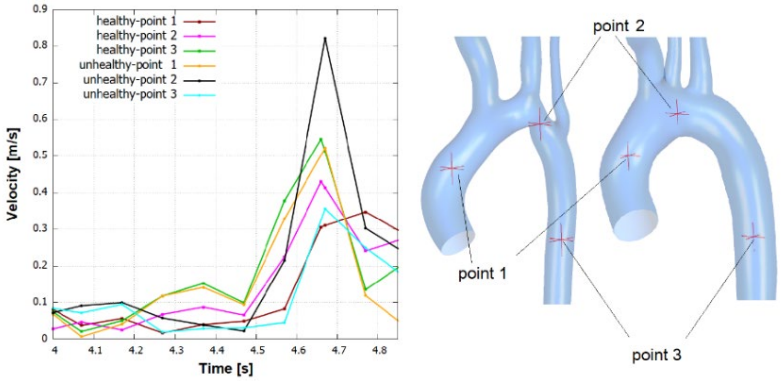

Figure 6 – Time profiles of mean velocity in the ascending and descending aorta for normal geometry and with coarctation

Pressure Distribution

Figure 7 shows the pressure distribution in a normal aorta and a coarctation aorta during peak systole. Healthy geometry is characterized by a smooth pressure decline from the ascending to the descending aorta, with a pressure differential of no more than 0.15 kPa.

With coarctation, a pronounced gradient develops: before the constriction, the pressure reaches ~1.8 kPa, while after the constriction, it drops to ~1.2 kPa. Thus, the peak differential is approximately 0.6 kPa, which is four times higher than in a normal aorta. This result indicates significant hemodynamic loading and is consistent with literature data on a critical increase in gradient in CoA [16, 23].

Figure 8 shows the pressure time profiles at the control points. In a normal aorta, the values remain similar, and the maximum gradient during the cycle is insignificant. In the model with coarctation, the differences become clearly expressed: the peak difference is recorded in systole, while in diastole the differences are smoothed out.

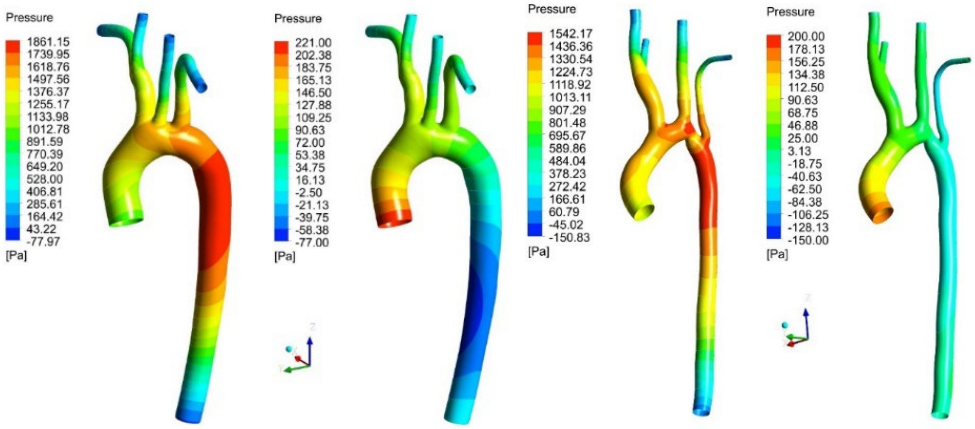

a b

Figure 7 – Pressure distribution in the normal aorta and with coarctation in the peak systole phase

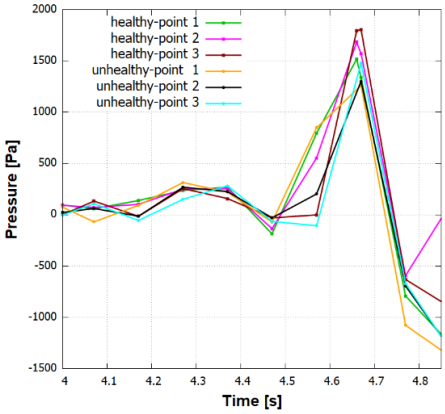

Figure 8 – Time profiles of pressure in the ascending and descending aorta for normal geometry and with coarctation

Wall Shear Stresses

Figure 9 shows the distribution of instantaneous wall shear stresses (WSS) for a normal aorta and one with coarctation. In normal geometry, WSS remains relatively uniform: maximum values are recorded in the curvature region, but their magnitude remains within the physiological range noted in the literature [24, 25].

In the coarctation model, a significant increase in WSS is observed in the constriction zone, where stresses

exceed background values by more than two times. Simultaneously, areas of reduced WSS develop behind the constriction, associated with recirculation and weakening of shear loads on the wall. This combination of high and low stresses is known to be a risk factor for the development of endothelial dysfunction and the progression of vascular pathologies.

Time-averaged shear stress confirms that the highest WSS values are achieved during peak systole. The cycle-averaged distribution (TAWSS) indicates that the normal aorta is characterized by smoothed values along the wall, whereas coarctation produces a localized peak in the narrowed area and an extended region of reduced TAWSS beyond it.

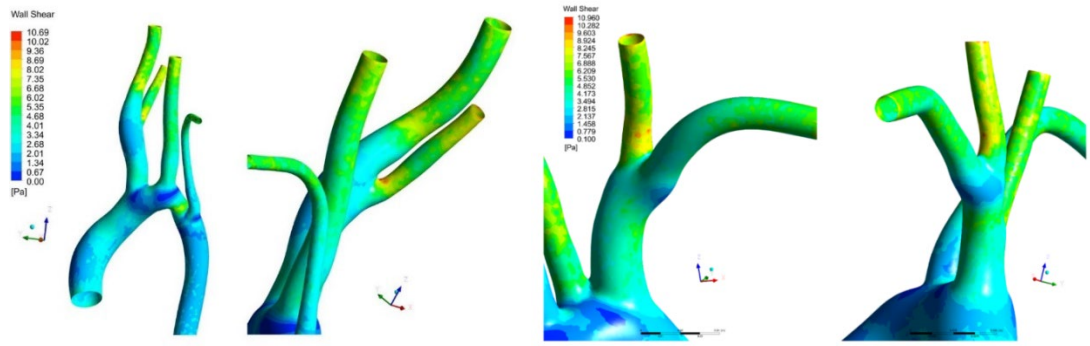

CoA Healthy

Figure 9 – Distribution of instantaneous wall shear stresses (WSS) in the normal aorta and with coarctation

Conclusion

This study presents a numerical simulation of hemodynamics in the thoracic aorta based on anatomically realistic geometry obtained from medical images. A comparison of a normal aorta and an aorta with coarctation revealed that the presence of stenosis significantly alters the blood flow structure and key hydrodynamic parameters.

The main differences are evident during peak systole, when blood flow velocity in the stenosis zone increases by 1.6 times compared to normal geometry. Simultaneously, a significant pressure differential develops between the ascending and descending aorta, reaching approximately 0.6 kPa, significantly exceeding values for a healthy aorta. Analysis of shear stress distribution revealed a sharp increase in WSS in the stenosis area and the appearance of extended zones of reduced TAWSS beyond it. This combination of factors can contribute to the progression of vascular pathologies and complicated disease progression.

The obtained results confirm the importance of considering the geometric features of the aorta in numerical modeling and demonstrate that CFD analysis can serve as a useful tool for assessing hemodynamic disturbances in coarctation. A promising direction for further research is to expand the model by taking into account the interaction between blood flow and the deformable vascular wall, which will allow for a more complete reflection of real physiological conditions.

References

1. Coogan, J. S., J. D. Humphrey, and C. A. Figueroa. “Computational Simulations of Hemodynamic Changes within Thoracic, Coronary, and Cerebral Arteries Following Early Wall Remodeling in Response to Distal Aortic Coarctation.” *Biomechanics and Modeling in Mechanobiology* 12, (2013): 79–93. https://doi.org/10.1007/s10237-012-0383-x.

2. Lantz, J., T. Ebbers, J. Engvall, and M. Karlsson. “Numerical and Experimental Assessment of Turbulent Kinetic Energy in an Aortic Coarctation.” *Journal of Biomechanics* 46, no. 11 (2013): 1851–1858. https://doi.org/10.1016/j.jbiomech.2013.04.028.

3. O'Rourke, M. F., and T. B. Cartmill. “Influence of Aortic Coarctation on Pulsatile Hemodynamics in the Proximal Aorta.” *Circulation* 44, no. 2 (1971): 281–292. https://doi.org/10.1161/01.cir.44.2.281.

4. Markl, M., W. Wallis, and A. Harloff. “Reproducibility of Flow and Wall Shear Stress Analysis Using Flow-Sensitive Four-Dimensional MRI.” *Journal of Magnetic Resonance Imaging* 33, no. 4 (2011): 988–994. https://doi.org/10.1002/jmri.22519.

5. Ha, H., J. Lantz, M. Ziegler, B. Casas, M. Karlsson, P. Dyverfeldt, and T. Ebbers. “Estimating the Irreversible Pressure Drop across a Stenosis by Quantifying Turbulence Production Using 4D Flow MRI.” *Scientific Reports* 7, (2017): 46618. https://doi.org/10.1038/srep46618.

6. Ha, H., G. B. Kim, J. Kweon, S. J. Lee, Y. H. Kim, D. H. Lee, D. H. Yang, and N. Kim. “Hemodynamic Measurement Using Four-Dimensional Phase-Contrast MRI: Quantification of Hemodynamic Parameters and Clinical Applications.” *Korean Journal of Radiology* 17, no. 4 (2016): 445–462. https://doi.org/10.3348/kjr.2016.17.4.445.

7. Reiter, G., U. Reiter, G. Kovacs, H. Olschewski, and M. Fuchsjäger. “Blood Flow Vortices along the Main Pulmonary Artery Measured with MR Imaging for Diagnosis of Pulmonary Hypertension.” *Radiology* 275, no. 1 (2015): 71–79. https://doi.org/10.1148/radiol.14140849.

8. Bakhshinejad, A., A. Baghaie, A. Vali, D. Saloner, V. L. Rayz, and R. M. D'Souza. “Merging Computational Fluid Dynamics and 4D Flow MRI Using Proper Orthogonal Decomposition and Ridge Regression.” *Journal of Biomechanics* 58 (2017): 162–173. https://doi.org/10.1016/j.jbiomech.2017.05.004.

9. Saitta, Simone, Selene Pirola, Filippo Piatti, Emiliano Votta, Federico Lucherini, Francesca Pluchinotta, Mario Carminati, Massimo Lombardi, Christian Geppert, Federica Cuomo, Carlos Alberto Figueroa, Xiao Yun Xu, and Alberto Redaelli. “Evaluation of 4D Flow MRI-Based Non-Invasive Pressure Assessment in Aortic Coarctations.” *Journal of Biomechanics* 94 (2019): 13–21. https://doi.org/10.1016/j.jbiomech.2019.07.004.

10. LaDisa, J. F. Jr., R. J. Dholakia, C. A. Figueroa, I. E. Vignon-Clementel, F. P. Chan, M. M. Samyn, J. R. Cava, C. A. Taylor, and J. A. Feinstein. “Computational Simulations Demonstrate Altered Wall Shear Stress in Aortic Coarctation Patients Treated by Resection with End-to-End Anastomosis.” *Congenital Heart Disease* 6, no. 5 (2011): 432–443. https://doi.org/10.1111/j.1747-0803.2011.00553.x.

11. Caballero, A. D., and S. Laín. “A Review on Computational Fluid Dynamics Modelling in Human Thoracic Aorta.” *Cardiovascular Engineering and Technology* 4 (2013): 103–130. https://doi.org/10.1007/s13239-013-0146-6.

12. Malvè, M., A. García, J. Ohayon, and M. A. Martínez. “Unsteady Blood Flow and Mass Transfer of a Human Left Coronary Artery Bifurcation: FSI vs. CFD.” *International Communications in Heat and Mass Transfer* 39, no. 6 (2012): 745–751. https://doi.org/10.1016/j.icheatmasstransfer.2012.04.009.

13. Shang, E. K., D. P. Nathan, S. R. Sprinkle, S. C. Vigmostad, R. M.Fairman, J. E. Bavaria, R.C. Gorman, J.H. Gorman III, K.B. Chandran, and B.M. Jackson. “Peak Wall Stress Predicts Expansion Rate in Descending Thoracic Aortic Aneurysms.” *Annals of Thoracic Surgery* 95 (2012): 593-598. https://doi.or/10.1016/j.athoracsur.2012.10.025.

14. Cunningham, K. S., and A. I. Gotlieb. “The Role of Shear Stress in the Pathogenesis of Atherosclerosis.” *Laboratory Investigation* 85, no. 1 (2005): 9–23. https://doi.org/10.1038/labinvest.3700215.

15. Pons, R., A. Guala, J. F. Rodríguez-Palomares, J. C. Cajas, L. Dux-Santoy, G. Teixidó-Tura, J. J. Molins, M. Vázquez, A. Evangelista, and J. Martorell. “Fluid–Structure Interaction Simulations Outperform Computational Fluid Dynamics in the Description of Thoracic Aorta Hemodynamics and in the Differentiation of Progressive Dilation in Marfan Syndrome Patients.” *Royal Society Open Science* 7 (2020): 191752. https://doi.org/10.1098/rsos.191752.

16. Ambrosi, D., A. Quarteroni, and G. Rozza, eds. *Modeling of Physiological Flows.* Milan: Springer-Verlag Italia, 2012.

17. Torii, R., J. Keegan, N. B. Wood, et al. “MR Image-Based Geometric and Hemodynamic Investigation of the Right Coronary Artery with Dynamic Vessel Motion.” *Annals of Biomedical Engineering* 38 (2010): 2606–2620. https://doi.org/10.1007/s10439-010-0008-4.

18. Jin, S., J. Oshinski, and D. P. Giddens. “Effects of Wall Motion and Compliance on Flow Patterns in the Ascending Aorta.” *Journal of Biomechanical Engineering* 125, no. 3 (2003): 347–354. https://doi.org/10.1115/1.1574332.

19. Johnston, B. M., P. R. Johnston, S. Corney, and D. Kilpatrick. “Non-Newtonian Blood Flow in Human Right Coronary Arteries: Steady State Simulations.” *Journal of Biomechanics* 37, no. 5 (2004): 709–720. https://doi.org/10.1016/j.jbiomech.2003.09.016.

20. Cho, Y. I., and K. R. Kensey. “Effects of the Non-Newtonian Viscosity of Blood on Flows in a Diseased Arterial Vessel. Part 1: Steady Flows.” *Biorheology* 28, no. 3–4 (1991): 241–262. https://doi.org/10.3233/bir-1991-283-415.

21. Wilson, N. M., A. K. Ortiz, and A. B. Johnson. “The Vascular Model Repository: A Public Resource of Medical Imaging Data and Blood Flow Simulation Results.” *Journal of Medical Devices* 7, no. 4 (2013): 040923. https://doi.org/10.1115/1.4025983.

22. Labroquere. *Navier–Stokes Computation with Num3sis – Poiseuille Flow and Backward Facing Step.*

23. Paisal, M. S. A., I. Taib, A. E. Ismail, A. M. Tajul Arifin, and N. Darlis. “An Analysis of Blood Pressure Waveform Using Windkessel Model for Normotensive and Hypertensive Conditions in Carotid Artery.” *Journal of Advanced Research in Fluid Mechanics and Thermal Sciences* 57, no. 1 (2020): 69–85.

24. Rodríguez-Palomares, J. F., L. Dux-Santoy, A. Guala, R. Kale, G. Maldonado, G. Teixidó-Turà, L. Galian, M. Huguet, F. Valente, L. Gutiérrez, T. González-Alujas, K. M. Johnson, O. Wieben, D. García-Dorado, and A. Evangelista. “Aortic Flow Patterns and Wall Shear Stress Maps by 4D-Flow Cardiovascular Magnetic Resonance in the Assessment of Aortic Dilatation in Bicuspid Aortic Valve Disease.” *Journal of Cardiovascular Magnetic Resonance* 20, no. 1 (2018): 28. https://doi.org/10.1186/s12968-018-0451-1.

25. Chetan, Devin, and Luc L. Mertens. “Challenges in Diagnosis and Management of Coarctation of the Aorta.” *Current Opinion in Cardiology* 37, no. 1 (2022): 115–122. https://doi.org/10.1097/HCO.0000000000000934.

26. Issakhov, A., A. Abylkassymova, and M. Sakypbekova. “Applications of Parallel Computing Technologies for Modeling the Mixed Convection in Backward-Facing Step Flows with the Vertical Buoyancy Forces.” *International Journal of Mathematics and Physics* 8, no. 2 (2017): 43–50. https://doi.org/10.26577/ijmph.2017.v8.i2.08

27. Issakhov, A., T. Yang, and A. Baitureyeva. “CFD Simulation of Pollution Dispersion from Thermal Power Plants in the Atmosphere.” *International Journal of Mathematics and Physics* 10, no. 1 (2019): 56–65. https://doi.org/10.26577/ijmph-2019-i1-8

Information about authors:

Alibek Issakhov (corresponding author) – PhD, Professor of the School of Applied Mathematics at Kazakh-British Technical University (Almaty, Kazakhstan, e-mail: Alibek.issakhov@gmail.com).

Uliana Timokhina – student at International School Haileybury (Almaty, Kazakhstan).

Jimin Na – student at International School Haileybury (Almaty, Kazakhstan).

Zhamilya Batyrbekova – student at International School Haileybury (Almaty, Kazakhstan).

Zhaniya Makasheva – student at International School Haileybury (Almaty, Kazakhstan).

Alina Akylova – student at International School Haileybury (Almaty, Kazakhstan).

Diyar Tokbayev – student at International School Haileybury (Almaty, Kazakhstan).